Alignment-free difference frequency light source tunable from 5 to 20 µm by mixing two independently tunable OPOs

Florian Mörz,* **Tobias Steinle, Heiko Linnenbank, Andy Steinmann, and Harald Giessen**

4th Physics Institute, University of Stuttgart, Research Center SCoPE, Pfaffenwaldring 57, 70569 Stuttgart, Germany
f.moerz@pi4.uni-stuttgart.de

Abstract: Tunable mid-infrared ultrashort lasers have become an essential tool in vibrational spectroscopy in recent years. They enabled and pushed a variety of spectroscopic applications due to their high brilliance, beam quality, low noise, and accessible wavelength range up to 20 µm. Many state-of-the-art devices apply difference frequency generation (DFG) to reach the mid-infrared spectral region. Here, birefringent phase-matching is typically employed, resulting in a significant crystal rotation during wavelength tuning. This causes a beam offset, which needs to be compensated to maintain stable beam pointing. This is crucial for any application. In this work, we present a DFG concept, which avoids crystal rotation and eliminates beam pointing variations over a broad wavelength range. It is based on two independently tunable input beams, provided by synchronously pumped parametric seeding units. We compare our concept to the more common DFG approach of mixing the signal and idler beams from a single optical parametric amplifier (OPA) or oscillator (OPO). In comparison, our concept enhances the photon efficiency of wavelengths exceeding 11 µm more than a factor of 10 and we still achieve milliwatts of output power up to 20 µm. This concept enhances DFG setups for beam-pointing-sensitive spectroscopic applications and can enable research at the border between the mid- and far-IR range due to its highly efficient performance.

1. Introduction

The application of ultrafast MIR lasers with high repetition rates for spectroscopy has enabled a variety of novel research topics, which have not been feasible before. Among many others, *in vitro* monitoring of structural processes in protein research at attomolar concentrations in far-field spectroscopy [1], or of individual protein complexes in near-field spectroscopy [2], monitoring the hydrogen diffusion into metal hydrides [3], or the characterization of novel materials for miniature optoelectronic devices in the fingerprint region [4–7] are just a few examples. The modern world is based on highly technical processes and their impact will further grow in search of solutions for renewable energy sources, environmentally friendly transportation, remote sensing, life sciences, or for the growing digitization. Research in these fields can significantly benefit from vibrational spectroscopy in the mid-infrared spectral region using ultrafast laser sources due to their excellent beam profile, high brilliance and power, low RMS and intensity noise and their excellent long-term stability [1,8–10]. Many state-of-the-art laser sources consist of multiple cascaded parametric frequency conversion stages, as this concept allows for a very broad tuning range from the near infrared up to 20 µm wavelength with high conversion efficiencies. Especially in recent years, there have been a vast variety of new devices based on MIR optical parametric oscillators (OPOs) [11–13], intrapulse difference frequency generation (DFG) [14], DFG between the signal and idler beams of an near-infrared optical parametric amplifier (OPA) or OPO [9,15–19], or supercontinuum-seeded DFGs [20,21]. High

output powers, large bandwidths, wide tuning ranges or high conversion efficiencies have been reported using many different nonlinear materials. However, there is a limiting issue in their application in measurement devices. In contrast to standard nonlinear crystals used for the NIR region, such as periodically-poled lithium niobate (PPLN), which allow for quasi phase-matching (QPM), crystals for DFG in the MIR region usually require angular phase-matching, with just a few exceptions (e.g. OP-GaP, OP-GaAs), but those are limited in phase-matching bandwidth and transparency range [12,22–26]. QPM crystals can be inserted into the beam path at 0° angle of incidence, thus the input beams do not experience any spatial beam offset over the useable wavelength range. In contrast, birefringent phase-matching requires the crystal angle to be carefully adjusted relative to the beam propagation direction for every wavelength change [27]. Depending on the utilized nonlinear crystal, this results in crystal rotations of up to 40°, causing a significant spatial offset of the output beam. To maintain the coupling into subsequent spectroscopic devices, this offset needs to be accurately compensated, requiring active electronic or time-consuming manual compensation or counter-rotating compensation optics, all of which impede the application of parametric MIR light sources.

In this publication, we present a DFG concept that circumvents angular tuning of the nonlinear crystal. We are able to use a fixed crystal angle over a broad tuning range, ranging from 9 to 20 µm wavelength, by decoupling the pumping and seeding units. This additional degree of freedom is achieved by applying an OPA seeded by a fiber-feedback OPO (FFOPO) as a pump source, and a second independently tunable FFOPO for seeding the DFG. Thus, active beam offset compensation becomes dispensable. Furthermore, we achieve a very stable and nearly constant photon efficiency in the range from 5 to 15 µm and achieve mW-level output power up to 20 µm. As a proof-of-concept, we compare our dual OPO/OPA DFG setup to a more commonly used DFG scheme between the signal and idler beams of a single OPA. This concept typically allows very high output power from about 5 to 10 µm, but suffers from decreasing performance above 10 to 12 µm, as long DFG wavelengths require close-lying pump and seed wavelengths. This is difficult to achieve for signal-idler approaches, as the OPO/OPA then needs to operate near degeneracy. In addition, the transparency of many DFG crystals decreases continuously between 10 and 20 µm, which enhances the effect of low input power. Briefly, in a standard signal and idler DFG scheme, both the DFG crystal, as well as the seeding unit simultaneously approach their performance limits, which in consequence sum up. Our goal is to circumvent these effects in order to efficiently generate radiation in the long wavelength region by decoupling the working points of the DFG and seeding units and to use a fixed crystal position to maintain stable beam pointing up to 20 µm. To provide a fair comparison, similar beam parameters, optics and the identical nonlinear crystal are used in both setups.

2. Experimental preparation

In order to circumvent the crystal rotation that is required for phase-matching, the input beams need to be independently tunable. The idea is as follows. In a signal-idler DFG setup, phase-matching is satisfied by adjusting the crystal angle according to a fixed set of input wavelengths, as mentioned earlier. Upon reversion, by fixing the crystal angle, phase-matching could be satisfied by choosing the correct input wavelengths independently of each other. We achieve this by using the amplified FFOPO signal as DFG pump beam and the second FFOPO signal as DFG seed beam. To ensure the temporal synchronization of the pump and seed pulses, both seeding units are synchronously pumped by the same Yb:KGW solid-state oscillator.

Figure 1 depicts the experimental setups used in this work. A fixed crystal angle is achieved by using the dual OPO/OPA setup shown in Fig. 1(a). We apply an Yb:KGW solid-state laser, providing 7 W power at a center wavelength of 1.039 µm, and 500 fs pulses at 40 MHz repetition rate, to synchronously pump the two independent seeding units. About 4 W pump power is applied in total to the amplified FFOPO, which is tuned from 1.45 to 1.6 µm with a maximum

output power of 1.2 W. A pump power of 2.3 W is applied to the second FFOPO, which is tuned from 1.6 to 1.95 μm with output powers ranging from 225 to 500 mW. The two beams are combined using a beam splitter and focused (f = 75 mm) into the crystal.
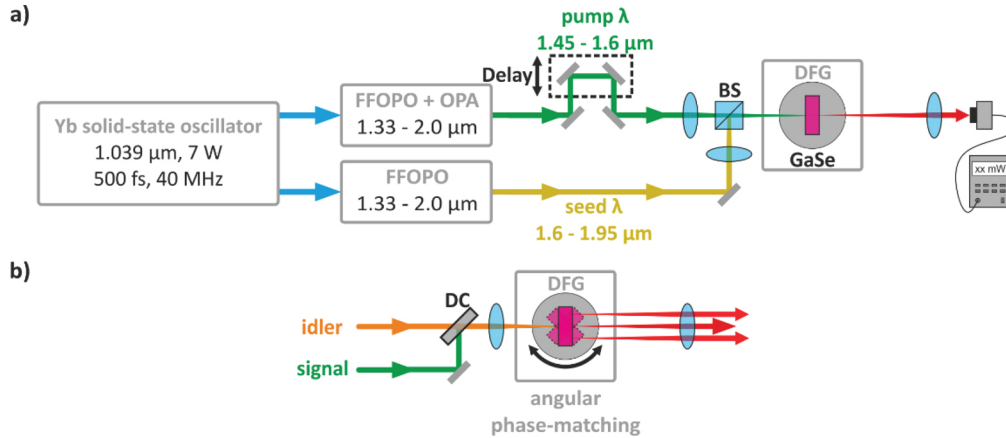

Fig. 1. Experimental setup. a) DFG setup based on two independently tunable fiber-feedback OPOs (FFOPO), pumped by the same Yb solid-state oscillator. The FFOPO providing the DFG pump beam (green) is additionally amplified by an OPA to enhance its output power. Both beams are combined by a polarizing beam splitter (BS) and focused into a 4-mm-long GaSe nonlinear crystal. b) DFG setup using signal and idler of a single post-amplified FFOPO. Angle tuning is required to satisfy the phase matching condition.

In Fig. 1(b), a standard DFG scheme between signal and idler beams is shown where both beams are provided by the same amplified FFOPO system, which is pumped with about 6 W total input power using the Yb:KGW oscillator. This setup is similar to the setup presented in [8,9]. The beams are combined using a dichroic mirror and focused into the nonlinear crystal using a lens with 75 mm focal length. Wavelength tuning is achieved by setting the signal wavelength in accordance with the desired DFG wavelength. Then the crystal angle relative to the beam direction is adjusted by monitoring the output power. The required crystal rotation causes a significant spatial beam offset of up to several hundred microns.

In this work, a 4-mm-long uncoated GaSe crystal (Eksma Optics) is used as a nonlinear medium in type-I phase-matching configuration. We chose this material as it offers a very high nonlinearity and a good figure of merit over a broad wavelength range and it is commercially available [28–30]. Furthermore, it exhibits a high damage threshold compared to other DFG crystals, which makes it very suitable for high input powers. Throughout the experiments, we used several GaSe crystals with lengths between 1 and 4 mm, including a 3.7-mm-long GaSSe crystal [31,32] from S. Sarkisov, Tomsk State University, Russia. We optimized the input beam sizes for every crystal. Experimentally, the best results have been achieved with the 4-mm-long GaSe crystal, although the results using the GaSSe were just slightly lower. Behind the crystal the DFG beam is collimated and spectrally separated from the pump and seed beams using a long-pass filter. The generated DFG power is measured behind the collimation optics and the long-pass filter using a thermal power meter (Ophir 3A sensor). The input power is measured in front of the focusing lenses. To derive the effectively applied input power, the reflected power from the input crystal facet is measured. It reaches about 25% of the applied power, in average. This is due to the very large external angle of about 35° relative to the beam direction of the GaSe crystal. For other tilt angles and for type-II phase-matching, the Fresnel losses can be even higher. For the calculation of the photon efficiency, the measured input power is corrected by the power reflected on the input facet.

3. Experimental results

First, we conducted measurements using our dual OPO/OPA DFG setup, which offers an additional degree of freedom resulting from the decoupled input beams, compared to the signal-idler DFG setup. It is optimized for a fixed crystal orientation over a broad wavelength range and allows the utilization of input wavelengths that avoid critical absorption windows and near-degeneracy-operation of the input light sources, in comparison to the more common signal-idler DFG. Initially, we determined a crystal angle that can be kept constant over the broadest possible tuning range, allowing maximum deviations of ±0.2°, which corresponds to the acceptance bandwidth $\Delta\theta = 0.4°$ of the utilized GaSe crystal. This has been carried out using the SNLO library. The crystal angle is determined by first analyzing the phase-matching angle in dependence on the required tuning range and applicable input wavelengths. We restricted the maximum input seed wavelength to 1.95 μm, whereas the minimum pump wavelength is 1.45 μm. Thus, we restricted the input wavelength range to the OPO/OPA signal wavelength range, as this enables high input power, using standard high-quality IR optics and avoiding critical absorptions. Iteratively, we then optimized the required set of input wavelengths with respect to the fixed crystal angle, DFG wavelength and optimum pump and seed power. Using GaSe crystals, this allows to fix the crystal angle for a tuning range from 9 to 20 μm. Below 9 μm the input wavelengths would exceed our self-set limits and we adjusted the crystal angle in order to stay within these limits. Of course, they can be extended depending on the seeding units.

In general, this concept can be applied to many other nonlinear crystals, as depicted in Fig. 2 for some of the most common MIR crystals assuming type-I phase-matching. Here, we plot the required rotation of the crystal angle for a given DFG wavelength. The semitransparent red areas show the acceptance bandwidth $\Delta\theta$ of the respective crystals (L = 4 mm). For simplicity, the spectral dependence of the acceptance bandwidth is neglected and the given values denote the median acceptance bandwidth. All values that are within the marked areas can be generated using a fixed crystal angle, but with varying efficiency depending on their deviation from the optimum angle, which is central in the semitransparent red areas. On the left side, the angle variation for the dual OPO/OPA DFG concept is shown, whereas the right side depicts the angle variation for a common DFG scheme between signal and idler beams from a single OPA. As illustrated, our concept theoretically allows minimizing the required crystal rotation within a 7 μm wide wavelength window using a GaSe crystal. Similar ranges can be achieved for other nonlinear crystals such as AgGaSe$_2$ and CdSe. The appropriate crystal can be chosen according to the desired application. Here, we were particularly interested in GaSe due to its broad transparency range and high damage threshold.

As a further benefit of the dual OPO/OPA DFG concept, the effective nonlinearity, the figure of merit [28,33], and the spatial walk-off also remain more constant for a constant crystal angle.

Next, we applied the calculated parameters for a GaSe crystal using the dual OPO/OPA DFG setup. In Fig. 3(b), the utilized set of input wavelengths is depicted. The input beams are tuned to these wavelengths with 0.3 nm precision. This configuration allows a constant external angle of 35°.

The fixation of the crystal angle is depicted in Fig. 3(c). For this measurement, we optimized the crystal angle for each wavelength to confirm ideal phase-matching conditions by monitoring the generated output power. In black, the calculated rotation versus DFG wavelength is shown, the experimentally measured values are given in red. In general, the measured values follow the calculations very well. Above 9 μm wavelength the crystal orientation remains nearly constant, as expected according to our design. Only 0.3° maximum rotation is measured from 11 to 20 μm, which is within the limit of the acceptance bandwidth of $\Delta\theta = 0.4°$.

We achieve a maximum output power of 13 mW at 7 μm wavelength. This corresponds to a photon efficiency of 5.3% using 1142 mW pump power and 174 mW seed power. The highest photon efficiency of 6.2% is measured at 11 μm. In general, the photon efficiency is close to
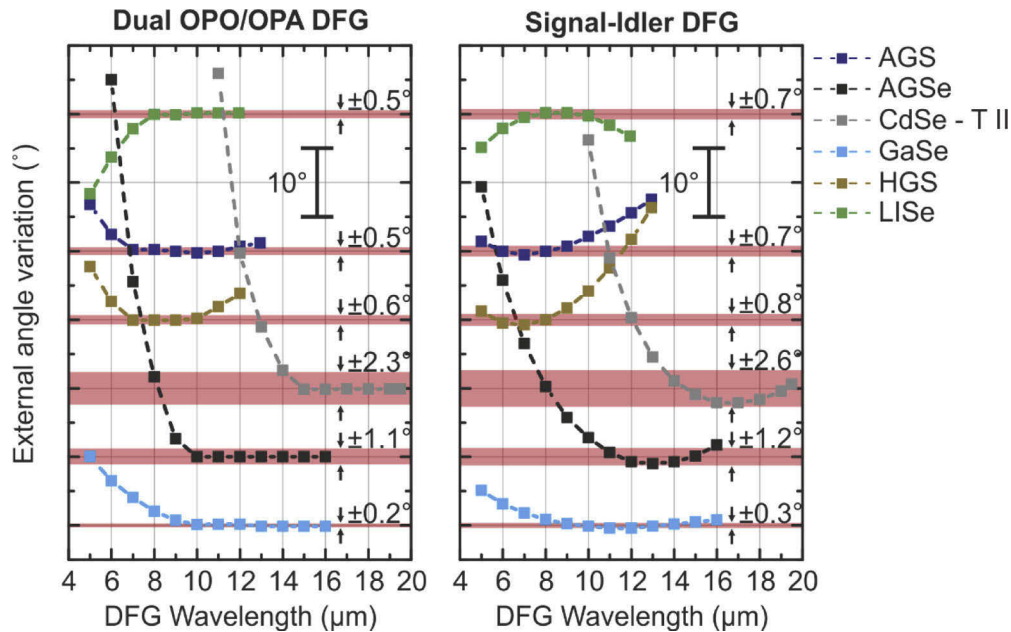
Fig. 2. External angle variation of different nonlinear crystals using the dual OPO/OPA DFG concept (two independent input beams) and a standard DFG between signal and idler beams for type-I phase-matching. Using decoupled input beams allows to fix the crystal angle in a specific wavelength range, being restricted by the input wavelength range (1.45–1.95 μm). The semitransparent areas depict the median acceptance bandwidth $\Delta\theta$ of the respective crystals. For simplicity, we calculated the acceptance bandwidth for 4-mm-long crystals, which is the length of the utilized GaSe crystal. If the plotted crystal angles are within the acceptance bandwidth, MIR radiation can be generated, without rotating the crystal. Using our concept enables a significant reduction of the angle variation within a broad bandwidth (>5 μm) for $AgGaS_2$, $AgGaSe_2$, CdSe (type-II phase-matching), and GaSe, thus minimizing beam pointing issues resulting from crystal rotation.

5% between 5 and 15 μm, being maximum between 11 and 14 μm. Between 15 and 20 μm the photon efficiency continuously decreases to just below 1% in consequence of the decreasing transparency of GaSe. About 0.5 mW power is still generated at 20 μm, despite limited crystal transparency [32,34]. Thus, the achieved output power and efficiency enable spectroscopic applications between 10 and 20 μm wavelength.

We also investigated the photon efficiency as a function of pump and seed power at 11.5 μm wavelength. Here, we observed a saturating photon efficiency in dependence on the applied pump power (190 mW constant seed power), whereas the efficiency remains continuously growing in dependence on the seed power (1000 mW constant pump power). We observed the identical behavior at 13.5 μm wavelength. In consequence, especially higher seed power is required for further enhancement of the photon efficiency. However, this would require a more powerful pump laser.

At 12 μm wavelength we measured the power stability within 45 minutes. We set the DFG power to 1.95 mW. Within those 45 minutes, the output power remained constant with an average of 1.935 mW. We measured a standard deviation of 38 μW, which corresponds to the intrinsic noise of the power meter, meaning no additional noise is adding up. This behavior is expected, as the DFG stability is given by the input beams. The input beams are optimized for excellent long-term stability reaching 0.1% rms, as described in [8].
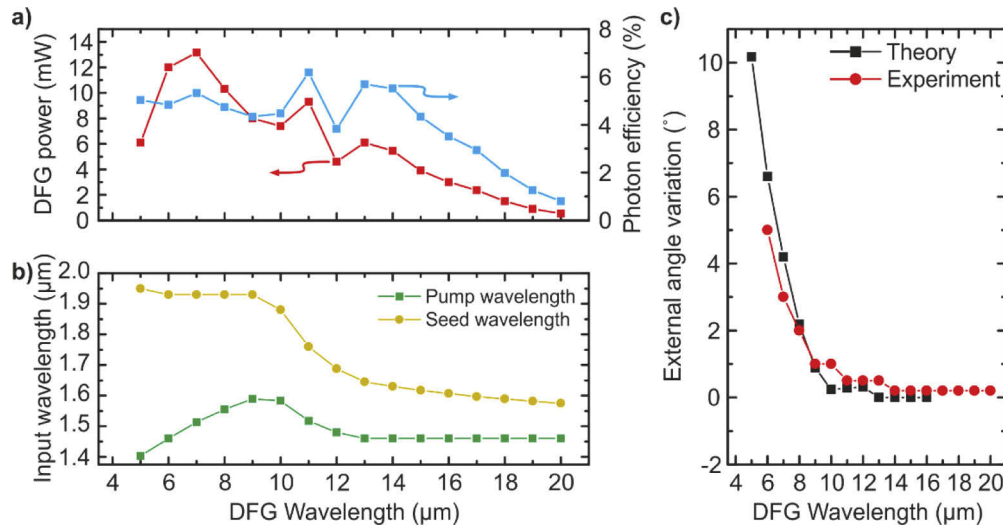
Fig. 3. a) Output power and photon efficiency for a constant phase-matching angle between 9 and 20 µm. Up to 13 mW output power and about 6% photon efficiency are achieved. The photon efficiency remains rather constant at around 5% between 5 and 15 µm. b) shows the required input wavelengths. For longer DFG wavelengths, input wavelengths between 1.7 and 1.6 µm, which is the optimum performance range of the seeding unit, are applied. c) External angle variation as measured in the experiment after optimization and as calculated. As shown, the angle remains nearly constant between 11 and 20 µm with negligible rotations of 0.3°. Below 9 µm, seed wavelengths > 2 µm would be required to keep the angle constant. As we limited the maximum seed wavelength to 1.95 µm the crystal angle needs to be adjusted at these wavelengths.

As mentioned before, we rotated the crystal to reach wavelengths between 5 and 9 µm. At this point, we realized another configuration, which we want to present briefly. By fixing one input wavelength and tuning the other input wavelength and the crystal angle instead, phase-matching can be satisfied as well. In this measurement, we fixed the seed wavelength at 1930 nm and generated MIR radiation from 6 to 9 µm. As this was only a narrow range, we repeated this configuration with a fixed seed wavelength of 1750 nm. Thus, we achieved a tuning range from 7 to 19 µm with reasonable output power up to 14 mW and 7.6% photon efficiency at 8 µm. Depending on the fixed wavelength, the MIR wavelength range could be shifted but such a detailed investigation is beyond the scope of the manuscript. However, this configuration might be interesting for more simplified DFG setups.

Next, we conducted similar measurements using DFG between signal and idler beams of the amplified FFOPO, as depicted in Fig. 1(b). Here, the signal wavelengths range from about 1.7 µm to 1.95 µm and the idler wavelengths are between 2.6 and 2.2 µm. In Fig. 4, the generated DFG power (Fig. 4(a)), as well as the photon efficiency (Fig. 4(b)) and the used input wavelengths (Fig. 4(c)) are shown. We also added the previously achieved results using the dual OPO/OPA DFG concept as a comparison. The signal-idler DFG provides superior output power between 5 and 10 µm wavelength, due to higher seed power available from the OPA idler. Up to 35 mW at 6 µm are achieved, using 813 mW signal and 277 mW idler power. This corresponds to a photon efficiency of 14.4%. In comparison to our dual OPO/OPA DFG concept, the photon efficiency remains higher up to 11 µm, reaching the maximum value of 15% at 7 µm wavelength.

Despite high power and a high photon efficiency in the range from 5 to 10 µm, the signal-idler DFG performance significantly drops towards longer wavelengths. However, as visible in Fig. 4(a),
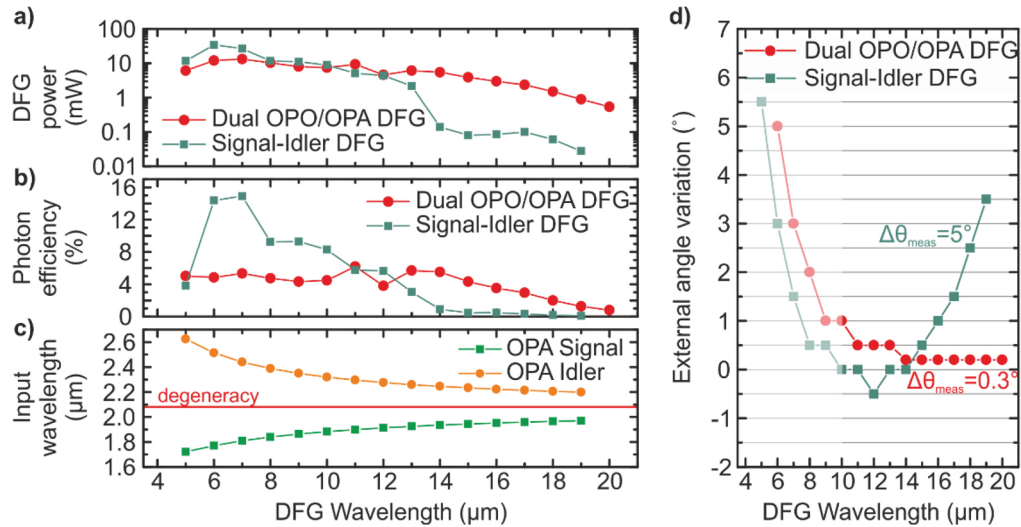
Fig. 4. a)-b) Comparison between our concept and a standard DFG setup using signal and idler beams. In the signal-idler DFG configuration an output power as high as 35 mW is achieved at 6 µm, corresponding to 14.4% photon efficiency. However, the performance significantly drops towards longer wavelengths. In contrast, the dual OPO/OPA DFG setup exhibits a very stable performance up to 20 µm with mW level output power, resulting from the optimum input wavelength range as shown in Fig. 3(a). c) Shows the input wavelengths for the signal-idler DFG configuration. d) The required external angle variation to achieve phase-matching is depicted. Precise angle tuning is required using the signal-idler scheme in contrast to the dual OPO/OPA DFG scheme, where nearly no tuning is applied.

we observe an unexpected drop in output power in the range from 14 and 16 µm. Indeed, this drop is traced back to an optical element in the amplified FFOPO, which attenuates the available pump and seed power between 1930 and 1950 nm due to a narrow absorption in the AR coating. The typically expected power can be estimated by assuming a continuously decreasing power from 13 to 17 µm. Nevertheless, the generated DFG power drops to about 100 µW towards 19 µm wavelength. At 20 µm no power can be measured. A qualitatively better comparison is given in Fig. 4(b), depicting the photon efficiency and thus accounting for the applied pump power. As visible, the signal-idler DFG becomes less efficient exceeding 12 µm. This is due to the near-degeneracy-operation of the amplified FFOPO, as visible in Fig. 4(c), which translates to the DFG setup leading to reduced efficiency. Using the dual OPO/OPA DFG approach this effect is avoided by tuning the pump and seed wavelengths to more optimum working points of the input sources, as depicted in Fig. 3(b). Besides, this concept also allows to avoid absorptions, which might appear in any AR coating, such as the previously mentioned, efficiently, due to the additional degree of freedom of independently tunable input wavelengths. In general, the dual OPO/OPA DFG provides a more constant efficiency and performance over the entire tuning range from 5 to 20 µm wavelength, whereas the signal-idler DFG allows higher maximum power and efficiency between 5 and 10 µm.

Besides comparing the photon efficiencies of the two setups, we also consider the ratio between the applied DFG pump (OPA signal) and seed (OPA idler) power, as the seed power remains disregarded in the photon efficiency calculations. In contrast to the very high parametric single pass gain observed in near-infrared crystals (e.g. PPLN), MIR DFG setups typically operate in the low gain regime and both pump and seed contribute linearly to the frequency conversion [33]. Thus, comparable pump and seed power is favorable. Using the signal-idler DFG, the mean ratio

between pump and seed power within the MIR tuning range is 2.5. In the dual OPO/OPA DFG concept, the mean ratio between pump and seed power reaches 4. Thus, with respect to the pump power, the dual OPO/OPA DFG performance could be further enhanced by applying higher seed power, which is currently limited by the available pump power of our Yb:KGW laser.

The most important difference between the two setups is depicted in Fig. 4(d), which shows the required angle rotation to cover a tuning range from 5 to 20 μm. Whereas the angle of the dual OPO/OPA DFG remains constant over a broad range, significant tuning is required using the signal-idler DFG. About 10° crystal rotation is required in total, and about 5° in the range, where the dual OPO/OPA DFG scheme provides a nearly constant angle ($\leq 0.3°$ rotation).

4. Summary

In conclusion, we present a versatile DFG scheme, which is based on independently tunable input beams. The system provides stable performance in a wavelength range from 5 to 20 μm with about 5% photon efficiency over the most part of the tuning range with several mW output power. Thus, the system provides enough power for most spectroscopic applications, including Fourier-transform infrared (FTIR) spectroscopy, scattering type scanning-near-field optical microscopy (SNOM), pump-probe experiments and many more. Moreover, the system avoids spatial beam offset due to rotation of the nonlinear DFG crystal over a broad wavelength range. Thus, beam offset compensation becomes dispensable. This concept can be transferred to different nonlinear materials and seeding units. Further power scaling is possible by increasing the power of the seeding unit, which is currently limited by the output power of the Yb:KGW laser. We believe that this concept is highly suited for spectroscopic measurements in the range from 10 to 20 μm, where beam pointing and available MIR power are limiting factors. Research in the field of superconducting materials, semiconductors, plasmonics, and life sciences can benefit from this concept.

Funding

Disclosures

The authors declare no conflicts of interest.

References

1. R. Semenyshyn, F. Mörz, T. Steinle, M. Ubl, M. Hentschel, F. Neubrech, and H. Giessen, "Pushing Down the Limit: In Vitro Detection of a Polypeptide Monolayer on a Single Infrared Resonant Nanoantenna," ACS Photonics **6**(11), 2636–2642 (2019).
2. I. Amenabar, S. Poly, W. Nuansing, E. H. Hubrich, A. A. Govyadinov, F. Huth, R. Krutokhvostov, L. Zhang, M. Knez, J. Heberle, A. M. Bittner, and R. Hillenbrand, "Structural analysis and mapping of individual protein complexes by infrared nanospectroscopy," Nat. Commun. **4**(1), 2890 (2013).
3. F. Sterl, H. Linnenbank, T. Steinle, F. Mörz, N. Strohfeldt, and H. Giessen, "Nanoscale Hydrogenography on Single Magnesium Nanoparticles," Nano Lett. **18**(7), 4293–4302 (2018).
4. C. Westermeier, A. Cernescu, S. Amarie, C. Liewald, F. Keilmann, and B. Nickel, "Sub-micron phase coexistence in small-molecule organic thin films revealed by infrared nano-imaging," Nat. Commun. **5**(1), 4101 (2014).
5. G. X. Ni, H. Wang, B. Y. Jiang, L. X. Chen, Y. Du, Z. Y. Sun, M. D. Goldflam, A. J. Frenzel, X. M. Xie, M. M. Fogler, and D. N. Basov, "Soliton superlattices in twisted hexagonal boron nitride," Nat. Commun. **10**(1), 4360 (2019).
6. K. Chaudhary, M. Tamagnone, X. Yin, C. M. Spägele, S. L. Oscurato, J. Li, C. Persch, R. Li, N. A. Rubin, L. A. Jauregui, K. Watanabe, T. Taniguchi, P. Kim, M. Wuttig, J. H. Edgar, A. Ambrosio, and F. Capasso, "Polariton nanophotonics using phase-change materials," Nat. Commun. **10**(1), 4487 (2019).
7. G. Németh, D. Datz, Á Pekker, T. Saito, O. Domanov, H. Shiozawa, S. Lenk, B. Pécz, P. Koppa, and K. Kamarás, "Near-field infrared microscopy of nanometer-sized nickel clusters inside single-walled carbon nanotubes," RSC Adv. **9**(59), 34120–34124 (2019).

8. F. Mörz, T. Steinle, A. Steinmann, and H. Giessen, "Multi-Watt femtosecond optical parametric master oscillator power amplifier at 43 MHz," Opt. Express **23**(18), 23960–23967 (2015).

9. T. Steinle, F. Mörz, A. Steinmann, and H. Giessen, "Ultra-stable high average power femtosecond laser system tunable from 1.33 to 20 μm," Opt. Lett. **41**(21), 4863–4866 (2016).

10. F. Mörz, R. Semenyshyn, T. Steinle, F. Neubrech, U. Zschieschang, H. Klauk, A. Steinmann, and H. Giessen, "Nearly diffraction limited FTIR mapping using an ultrastable broadband femtosecond laser tunable from 1.33 to 8 μm," Opt. Express **25**(26), 32355–32363 (2017).

11. B. Metzger, B. Pollard, I. Rimke, E. Büttner, and M. B. Raschke, "Single-step sub-200 fs mid-infrared generation from an optical parametric oscillator synchronously pumped by an erbium fiber laser," Opt. Lett. **41**(18), 4383–4386 (2016).

12. L. Maidment, P. G. Schunemann, and D. T. Reid, "Molecular fingerprint-region spectroscopy from 5 to 12 μm using an orientation-patterned gallium phosphide optical parametric oscillator," Opt. Lett. **41**(18), 4261–4264 (2016).

13. S. Chaitanya Kumar, J. Krauth, A. Steinmann, K. T. Zawilski, P. G. Schunemann, H. Giessen, and M. Ebrahim-Zadeh, "High-power femtosecond mid-infrared optical parametric oscillator at 7 μm based on CdSiP$_2$," Opt. Lett. **40**(7), 1398–1401 (2015).

14. H. Timmers, A. Kowligy, A. Lind, F. C. Cruz, N. Nader, M. Silfies, G. Ycas, T. K. Allison, P. G. Schunemann, S. B. Papp, and S. A. Diddams, "Molecular fingerprinting with bright, broadband infrared frequency combs," Optica **5**(6), 727–732 (2018).

15. M. Beutler, I. Rimke, E. Büttner, V. Badikov, D. Badikov, and V. Petrov, "Efficient femtosecond 50 MHz repetition rate mid-IR source up to 17 μm by difference-frequency generation in AgGaSe$_2$," Proc. SPIE **8964**, 89640D (2014).

16. M. Beutler, I. Rimke, E. Büttner, P. Farinello, A. Agnesi, V. Badikov, D. Badikov, and V. Petrov, "Difference-frequency generation of ultrashort pulses in the mid-IR using Yb-fiber pump systems and AgGaSe$_2$," Opt. Express **23**(3), 2730–2736 (2015).

17. M. Beutler, I. Rimke, E. Büttner, V. Petrov, and L. Isaenko, "Difference-frequency generation of fs and ps mid-IR pulses in LiInSe$_2$ based on Yb-fiber laser pump sources," Opt. Lett. **39**(15), 4353–4355 (2014).

18. M. Beutler, I. Rimke, E. Büttner, V. Petrov, and L. Isaenko, "Femtosecond mid-IR difference-frequency generation in LiInSe$_2$," Opt. Mater. Express **3**(11), 1834–1838 (2013).

19. M. Beutler, I. Rimke, E. Büttner, V. Panyutin, and V. Petrov, "80-MHz difference-frequency generation of femtosecond pulses in the mid-infrared using GaS$_{0.4}$Se$_{0.6}$," Laser Phys. Lett. **10**(7), 075406 (2013).

20. F. Keilmann and S. Amarie, "Mid-infrared frequency comb spanning an octave based on an er fiber laser and difference-frequency generation," J. Infrared, Millimeter, Terahertz Waves **33**(5), 479–484 (2012).

21. Y. Yao and W. H. Knox, "Broadly tunable femtosecond mid-infrared source based on dual photonic crystal fibers," Opt. Express **21**(22), 26612–26619 (2013).

22. N. Leindecker, A. Marandi, R. L. Byer, K. L. Vodopyanov, I. Hartl, M. Fermann, and P. G. Schunemann, "Ovtave-spanning ultrafast OPO with 2.6-6.1 μm instantaneous bandwidth pumped by femtosecond Tm-fiber laser," Opt. Express **20**(7), 7046–7053 (2012).

23. K. L. Vodopyanov, E. Sorokin, I. T. Sorokina, and P. G. Schunemann, "Mid-IR frequency comb source spanning 4.4–5.4 μm based on subharmonic GaAs optical parametric oscillator," Opt. Lett. **36**(12), 2275–2277 (2011).

24. K. L. Vodopyanov, I. Makasyuk, and P. G. Schunemann, "Grating tunable 4 - 14 μm GaAs optical parametric oscillator pumped at 3 μm," Opt. Express **22**(4), 4131–4136 (2014).

25. K. L. Vodopyanov, O. Levi, P. S. Kuo, T. J. Pinguet, J. S. Harris, M. M. Fejer, B. Gerard, L. Becouara, and E. Lallier, "Optical parametric oscillation in quasi-phasematched GaAs," Opt. Lett. **29**(16), 1912–1914 (2004).

26. T. Skauli, K. L. Vodopyanov, T. J. Pinguet, A. Schober, O. Levi, L. A. Eyres, M. M. Fejer, J. S. Harris, B. Gerard, L. Becouarn, E. Lallier, and G. Arisholm, "Measurement of the nonlinear coefficient of orientation-patterned GaAs and demonstration of highly efficient second-harmonic generation," Opt. Lett. **27**(8), 628–630 (2002).

27. R. W. Boyd, *Nonlinear Optics 3rd Edition* (Academic Press, 2008).

28. V. Petrov, "New applications of chalcopyrite crystals in nonlinear optics," Phys. Status Solidi Curr. Top. Solid State Phys. **14**(6), 1600161 (2017).

29. K. L. Vodopyanov, L. A. Kulevskii, V. G. Voevodin, A. I. Gribenyukov, K. R. Allakhverdiev, and T. A. Kerimov, "High efficiency middle IR parametric superradiance in ZnGeP$_2$ and GaSe crystals pumped by an erbium laser," Opt. Commun. **83**(5-6), 322–326 (1991).

30. K. L. Vodopyanov and L. A. Kulevskii, "New dispersion relationships for GaSe in the 0.65 - 18 μm spectral region," Opt. Commun. **118**(3-4), 375–378 (1995).

31. S. Das, C. Ghosh, O. G. Voevodina, Y. M. Andreev, and S. Y. Sarkisov, "Modified GaSe crystal as a parametric frequency converter," Appl. Phys. B **82**(1), 43–46 (2006).

32. V. Petrov, V. L. Panyutin, A. Tyazhev, G. Marchev, A. I. Zagumennyi, F. Rotermund, F. Noack, K. Miyata, L. D. Iskhakova, and A. F. Zerrouk, "GaS$_{0.4}$Se$_{0.6}$: Relevant properties and potential for 1064 nm pumped mid-IR OPOs and OPGs operating above 5 μm," Laser Phys. **21**(4), 774–781 (2011).

33. V. Petrov, "Frequency down-conversion of solid-state laser sources to the mid-infrared spectral range using non-oxide nonlinear crystals," Prog. Quantum Electron. **42**, 1–106 (2015).

34. K. L. Vodopyanov, "Parametric generation of tunable infrared radiation in ZnGeP$_2$ and GaSe pumped at 3 μm," J. Opt. Soc. Am. B **10**(9), 1723–1729 (1993).